



1 **Measurement report: Intra-, inter-annual variability and**  
2 **source apportionment of VOCs during 2018-2020 in**  
3 **Zhengzhou, Central China**

4 Shijie Yu <sup>a,b</sup>, Shenbo Wang<sup>b,c</sup>, Ruixin Xu <sup>b,c</sup>, Dong Zhang <sup>a,b</sup>, Meng Zhang <sup>e</sup>,  
5 Fangcheng Su<sup>b,c</sup>, Ruiqin Zhang <sup>b,c\*</sup>, Lingling Wang <sup>d\*</sup>

6 *a. College of Chemistry, Zhengzhou University, Zhengzhou 450001, China*

7 *b. Institute of Environmental Sciences, Zhengzhou University, Zhengzhou 450001, China*

8 *c. School of Ecology and Environment, Zhengzhou University, Zhengzhou 450001, China*

9 *d. Environmental Monitoring Center of Henan Province, Zhengzhou 450000*

10 *e. Pingdingshan Ecological Environment Monitoring Center of Henan Province, Pingdingshan*  
11 *467000, China*

12

13 Correspondence to: Ruiqin Zhang ( [rqzhang@zzu.edu.cn](mailto:rqzhang@zzu.edu.cn) ) and Lingling Wang (  
14 [Lindaw2007@126.com](mailto:Lindaw2007@126.com) )

15



## 16 **Abstract:**

17 Ambient volatile organic compounds (VOCs) were measured continuously to  
18 investigate their characteristics, sources, atmospheric oxidation capacity (AOC) and  
19 chemical reactivity from January 2018 to December 2020 at an urban site in  
20 Zhengzhou, China. In this study, the total concentration of observed VOCs was  
21  $38.2 \pm 15.6$  ppbv during the sampling period, with the characteristics that alkanes were  
22 the major VOC species, accounting for 60% of total VOCs. During the sampling  
23 period, the inter-annual variation of VOCs gradually reduced from  $45.0 \pm 25.2$  ppbv in  
24 2018 to  $36.7 \pm 22.0$  ppbv in 2019, and to  $30.5 \pm 15.4$  ppbv in 2020. Ethane, ethene, and  
25 propane were the top three abundant species during the three-year observation period.  
26 The results showed that total AOC, dominated by OH radical reactions, was  $7.4 \times 10^7$   
27 molecules  $\text{cm}^{-3} \text{s}^{-1}$ . The total OH reactivity was  $45.3 \text{ s}^{-1}$ , and mainly contributed by  
28 NO<sub>x</sub>. The AOC and •OH reactivity exhibited well-defined seasonal and inter-annual  
29 patterns. Therefore, the control strategy should focus on key species among  
30 inter-annual and seasonal variations. Meanwhile, diagnostic ratios of VOC species  
31 indicated VOCs in Zhengzhou were greatly affected by vehicle emissions and  
32 liquefied petroleum gas/natural gas (LPG/NG). Positive matrix factorization analysis  
33 showed six sources were identified, consisting of industrial sources, solvent use,  
34 vehicle exhaust, LPG/NG, coal+biomass burning and biogenic sources. Vehicle  
35 emissions, solvent use and LPG/NG made the largest contributions to VOC emission  
36 in all three years. The proportion of the contribution of vehicle emissions and  
37 LPG/NG has increased with each passing year. However, the proportion of industrial  
38 and solvent sources presented a decreasing trend, which is speculated that the policy  
39 control effect is remarkable. The effect of VOCs on ozone formation suggests that  
40 vehicle emission and solvent utilization were still key sources. Therefore, it is  
41 necessary to formulate effective strategies for reducing ground-level O<sub>3</sub>, and those  
42 sources mentioned above should be strictly controlled by the regulatory authorities.

43  
44



## 45 1. Introduction

46 In recent years, regional atmospheric pollution has occurred frequently in the world.  
47 Many areas are suffering from severe haze episodes in autumn and winter, and O<sub>3</sub>  
48 pollution in summer (Li et al., 2019; Yan et al., 2018; Zhang et al., 2018). As volatile  
49 organic compounds (VOCs) are the important precursor of secondary pollutants such  
50 as ozone (O<sub>3</sub>) and secondary organic aerosol (SOA), the study of VOCs is booming  
51 from the scientific community and governing bodies (Liu et al., 2019a; Song, et al.,  
52 2019c; Xu et al., 2017).

53 VOCs cover a large variety of species, and the chemical reactivity of each  
54 species varies greatly. Thus, VOC characteristics and active substance identification  
55 are a research priority. Alkanes were the dominant VOC species in many regions,  
56 while aromatics and alkenes were the largest contributors of ozone formation  
57 potential (OFP) (Li et al., 2019b; Yan et al., 2017). Yang et al. (2019) suggested that  
58 alkanes were the dominant group with 42% of the VOCs concentration, and C<sub>2</sub>-C<sub>3</sub>  
59 hydrocarbons were the dominant substance in Wuhan. Huang and Hsieh (2019)  
60 studied the maximum incremental reactivity (MIR) and propylene-equivalent (PE)  
61 concentration, reporting toluene was the largest potential contributor to OFP, and  
62 industrial emissions contributed nearly 60% to OFP. Considering the complex  
63 composition of VOCs in the atmosphere, it is difficult to determine the sources of  
64 VOCs. Receptor models are widely used to apportion the source contributions of  
65 VOCs, including positive matrix factorization (PMF), chemical mass balance, and  
66 principal component analysis. In China, traffic emissions are often the main source of  
67 VOCs, particularly in major metropolitan areas (Li et al., 2019; Liu et al., 2019; Song,  
68 et al., 2019b). Moreover, industrial process and solvent utilization had remarkable  
69 influence on VOC emission (Hui et al., 2019; Mo et al., 2017). Biogenic sources also  
70 cannot be ignored due to the high reactivity, which contributed 5-20% of VOC  
71 emission (Wu et al., 2016). In addition to the study of VOCs characteristics and  
72 source apportionment, the analysis of atmospheric oxidation characteristics is a



73 current research hotspot. The variations in the AOC not only affect the O<sub>3</sub> level in  
74 summer but also greatly impact the generation of secondary particles throughout the  
75 entire year (Prinn, 2003). However, most of the related studies in China focused on  
76 metropolitan areas, such as Beijing-Tianjin-Hebei (BTH) region (Gu et al., 2019b),  
77 Pearl River Delta region (Zhang et al., 2015), and Yangtze River Delta region (Xu et  
78 al., 2017; Zheng et al., 2020), but less research was carried on the heavily polluted  
79 central plains. Meanwhile, previous studies are frequently used monitoring data in a  
80 short time range, which can not reflect the comprehensive VOC pollution  
81 characteristics in a region. Therefore, large-scale investigations should be  
82 concentrated in central plains of China that has received limited attention in the past.

83 As the political and cultural center of Henan province, Zhengzhou has more than  
84 10 million permanent residents and 4.0 million private vehicles in 2019 (Gu et al.,  
85 2019a). This area is confronted with severe haze episodes and photochemical  
86 pollution due to emit huge amounts of air pollutants (Li et al., 2020b). As a hot spot,  
87 Zhengzhou has conducted a lot of research on air pollution, but many of those were  
88 only focused on particulate matter (Jiang et al., 2018; Wang et al., 2019). There are  
89 fewer studies on VOCs, especially the longer sampling time frames and seasonal  
90 measurements in Zhengzhou. Through the adjustment of policies together with the  
91 optimization of energy structure, the characteristics and sources of VOCs may be  
92 significantly affected by a number of mitigation measures in recent years due to the  
93 adjustment of policies and the optimization of energy structure. Therefore, it is  
94 necessary to identify local VOC pollution characteristics based on a long time series  
95 of monitoring data, which can provide a reference for the formulation of local air  
96 pollution control measures.

97 To deepen the understanding of VOC pollution characteristics, chemical  
98 reactivity and source contribution, three-year continuous VOCs data was measured  
99 using online instruments in Zhengzhou from 2018 to 2020. The aims of this research  
100 are: (1) analyze the variation characteristics of VOCs in Zhengzhou, including diurnal,  
101 seasonal, and annual changes; (2) quantify the contribution of sources among intra-,  
102 inter-annual variations and identify the locations of VOC sources; (3) parameterize



103 AOC and speciate OH reactivity; and (4) assess ozone formation by MIR and PE  
104 analysis.  
105

## 106 **2. Methodology**

### 107 **2.1 Site and measurements**

108 The observation period of this study is from January 2018 to December 2020.  
109 VOC samples are collected at an urban site (34°45'N, 113°41'E) in the Department of  
110 Environmental Protection of Henan Province. The surrounding environment was  
111 mainly commercial and residential district, and there are traffic sources but no large  
112 industrial source, which can represent a typical urban environment in Zhengzhou (Fig.  
113 1).

114 The VOC species are continuously monitored by using an auto-GC system  
115 (AMA Instruments GmbH, Germany). The specific information of this system was  
116 described in Zou et al. (2015). The 57 VOC species (including 29 alkanes, 10 alkenes,  
117 1 alkyne, and 17 aromatics) are calibrated by the VOC Standards of U.S. EPA PAMS  
118 mixture (Spectra Gases, USA) before monitoring. During the observation period, zero  
119 and span gas checks (PAMS calibration gases) were conducted monthly using the  
120 5-point method, together with the adjustment of retention time. Data quality control of  
121 this instrument is detailed in our previous study (Ren et al., 2020). The correlation  
122 coefficient usually varied from 0.990 to 0.999, and the detection limits ranged from  
123 0.02 to 0.12 ppbv, as shown in Table S1.

124 Meteorological data, such as atmospheric temperature (T), relative humidity  
125 (RH), Ultra-Violet Ray (UV), precipitation (Pr), the planetary boundary layer height  
126 (PBL), wind speed (WS) and direction (WD) were obtained from the surface  
127 meteorological station of Henan monitoring center. Other trace gases datasets such as  
128 the hourly NO, NO<sub>2</sub>, CO, O<sub>3</sub>, SO<sub>2</sub>, and fine particles (PM<sub>2.5</sub>) were obtained from the  
129 ambient air quality observation station of Yanchang, which is about 2 km away from



130 the VOC monitoring station.

## 131 **2.2 Positive Matrix Factorization model**

132 In this paper, the model of U.S. EPA PMF 5.0 was used to identify the sources  
133 and their contributions to VOCs (Gao et al., 2018; Norris et al., 2014; Song et al.,  
134 2019a, 2019b; Yadav et al., 2019), and the details were showed in the supplement  
135 (Text S1).

## 136 **2.3 Relative reactivity of VOCs**

137 To better understand the role of VOCs in the formation of troposphere O<sub>3</sub>, OFP  
138 and the PE concentration are investigated to analyze the chemical reactivity of VOC  
139 species (Carter, 1994; Atkinson and Arey, 2003), and the detailed operation were  
140 described in the supplementary materials (Text S2).

## 141 **2.4 Atmospheric oxidation capacity and speciated oxidant 142 reactivity**

143 AOC is defined as the sum of the respective oxidation rates of primary pollutants  
144 (e.g., CO, CH<sub>4</sub>, and VOCs) by the oxidants (e.g., OH, NO<sub>3</sub> and O<sub>3</sub>), and it can be  
145 calculated by the Eq. (1) (Elshorbany et al., 2009; Xue et al., 2016).

$$146 \quad \text{AOC} = \sum_i k_{Y_i} [X] [Y_i] \quad (3)$$

147 Where  $[X]$  and  $[Y_i]$  are the number concentrations of molecule oxidant X and  $Y_i$ ,  
148 respectively; and  $k_{Y_i}$  is the bi-molecular rate constant of molecule  $Y_i$  with oxidant X  
149 (Zhu et al., 2020). In this paper, the reduced substances only included 57 PAMS  
150 (provided by Spectra Gases Inc., USA) and CO. The oxidants only included •OH,  
151 NO<sub>3</sub> and O<sub>3</sub> radicals. And the concentration OH and NO<sub>3</sub> radicals was estimated from  
152 parameterization methods via Eq. (4) and Eq. (5) (Carter, 1994; Warneke, 2004).

$$153 \quad [\text{OH}] = a \times (J_{\text{O}^1\text{D}})^{\alpha} \times (J_{\text{NO}_2})^{\beta} \times \frac{b \times [\text{NO}_2] + 1}{c \times [\text{NO}_2]^2 + d \times [\text{NO}_2] + 1} \quad (4)$$



154 Where  $J_{O3}$  and  $J_{NO2}$  are measured photolysis frequency ( $s^{-1}$ ) of ozone and  $NO_2$ ,  
155 respectively. The value of a, b, c,  $\alpha$ ,  $\beta$  is  $4.1 \times 10^9$ , 140, 0.41, 1.7, 0.83 and 0.19,  
156 respectively (Yang et al., 2019).

157  $NO_3$  concentration in the atmosphere is based on the steady-state assumption  
158 (Liebmann et al., 2018).

$$159 \quad [NO_3] = \frac{k_{NO_2} \times [NO_2] \times [O_3]}{J_{NO_3} + J_{NO+NO_3} \times [NO] + \sum_i k_{NO_3+VOC_i} \times [VOC_i]} \quad (5)$$

160 Where  $J_{NO_3}$  is the measured photolysis frequency ( $s^{-1}$ ) of  $NO_3$ . The rate  
161 coefficients for  $NO_2-O_3$  ( $k_{NO_2+O_3}$ ) and  $NO-NO_3$  ( $k_{NO+NO_3}$ ) were obtained by Atkinson  
162 et al. (2004). A detailed description of the calculation processes of OH and  $NO_3$  have  
163 been provided in previous study (Yang et al., 2021).

164 Additionally, OH reactivity is another indicator of atmospheric oxidation. It is  
165 the inverse of the OH lifetime and defined as the product of the rate coefficients and  
166 the concentrations of the reactants with OH. OH reactivity is calculated by Eq. (6)  
167 (Mao et al., 2010):

$$168 \quad \text{OH reactivity} = \sum k_{OH+VOC_i} \times [VOC_i] + k_{OH+CO} \times [CO] + k_{OH+NO} \times [NO] + k_{OH+NO_2} \times [NO_2] \\ 169 \quad + k_{OH+SO_2} \times [SO_2] + k_{OH+O_3} \times [O_3] + k_{OH+other} \times [other] \quad (6)$$

170 Where  $[X_i]$  is the concentration of species (e.g., CO,  $NO_x$ ,  $SO_2$  and VOCs), and  
171 the rate coefficients  $k_{OH}$  (in  $cm^3 \text{ molecule}^{-1} s^{-1}$ ) represents the corresponding reaction  
172 rate coefficients.

## 173 2.5 CPF analysis

174 The CPF was developed to identify potential source contributions by using the  
175 PMF source contribution solution, coupled with the account of wind direction (Guo et  
176 al., 2011; Hsu et al., 2018; Wu et al., 2016). The CPF is defined as:

$$CPF = \frac{m_{\Delta\theta}}{n_{\Delta\theta}}$$

177 Where  $m_{\Delta\theta}$  is the number of appearances from wind sector  $\Delta\theta$  (each is  $22.5^\circ$ )  
178 that exceeds the concentration threshold (75th percentile of each source contribution)  
179 and  $n_{\Delta\theta}$  is the total number of occurrence in the same wind sector. Weak winds ( $< 1.5$



180 m s<sup>-1</sup>) were excluded from the calculation because of their difficulty in defining the  
181 wind direction (Zheng et al., 2018).

## 182 **3. Results and discussion**

### 183 **3.1 Characteristics of VOCs in Zhengzhou**

#### 184 **3.1.1 concentrations and compositions of VOCs**

185 Average ambient VOC concentrations and chemical species measured in  
186 Zhengzhou are shown in Table S2. The annual average concentration of VOCs was  
187 38.2±15.6 ppbv, close to the concentrations in Langfang (33.4 ppbv) (Song et al.,  
188 2019a) and Wuhan (32.6 ppbv) (Yang et al., 2019), lower than that in Nanjing (43.5  
189 ppbv) (An et al., 2014), Guangzhou (42.7 ppbv) (Zou et al., 2015), Mexico (84.0 ppbv)  
190 (Garzn et al., 2015), and higher than that in Guilin (23.7 ppbv) (Zhang et al., 2019),  
191 London UK (22.2 ppbv) (Schneidmesser et al., 2010) and Metropolitan Vancouver  
192 (19.2 ppbv) (Xiong et al., 2020). Alkanes were the major components of VOCs with a  
193 mean concentration of 23.0±19.5 ppbv, accounting for 60% of total VOC  
194 concentration, followed by alkenes (19%), aromatics (14%), and alkynes (7%). Many  
195 previous studies have found that alkanes were the dominant group (Fu et al., 2020; Gu  
196 et al., 2020), similar to that in Zhengzhou.

197 To clarify the characteristics of VOC emission sources, Table 1 lists the  
198 concentrations of the 20 most abundant species, accounting for 90% of the VOCs.  
199 During the sampling period (2018-2020), the most important VOC species in  
200 Zhengzhou were ethane (8.8±5.0 ppbv), ethylene (4.7±4.0 ppbv), propane (4.2±2.5  
201 ppbv), acetylene (2.6±3.3 ppbv), and n-butane (2.3±1.7 ppbv). In general, C<sub>2</sub>-C<sub>4</sub>  
202 species are closely related to vehicular exhausts, coal burning, and LPG (Hui et al.,  
203 2021; Zhang, et al. 2020). Among the most abundant 20 VOC species, half of them  
204 were alkanes, occupying 91% of the total alkanes measured. The C<sub>2</sub>-C<sub>3</sub> alkanes are  
205 mainly originated from LPG, while C<sub>4</sub>-C<sub>5</sub> alkanes are considered as the tracer for



206 vehicle emissions (Fan et al., 2021). The most abundant alkene species were ethylene,  
207 propene, isoprene, and 1-butene, representing 93% of the total alkanes. C<sub>2</sub>-C<sub>4</sub> alkenes  
208 mainly come from vehicle exhausts and LPG (Zhang et al., 2015), whereas isoprene is  
209 a typical biogenic tracer (Maji et al., 2020). There are five aromatics in the 20 most  
210 abundant species, including BTEX (benzene, toluene, ethyl-benzene, and xylenes)  
211 and styrene. Those aromatics are the most frequently observed aromatic compounds  
212 in urban areas, which are originated from vehicle exhausts, industrial processes,  
213 solvent usage, and combustion sources (Hui et al., 2019).

### 214 **3.1.2 Inter-annual variation of VOCs**

215 The inter-annual average concentrations and contributions of VOCs during 2018  
216 to 2020 are shown in Table S2. The inter-annual variation of VOCs gradually reduced  
217 as follows: 45.0±25.2 ppbv (in 2018), 36.7±22.0 ppbv (in 2019), and 30.5±15.4 ppbv  
218 (in 2020). The decrease trend of VOCs could be attributed to the increasingly  
219 stringent policies for emission reduction and the influence of COVID-19 lockdown on  
220 air quality in 2020 (Wang et al., 2021a).

221 The concentrations of the 20 most abundant species are listed in Table 1. Ethane,  
222 ethene, and propane were the top three abundant species during all three years, which  
223 is speculated that LPG and vehicular exhausts had a significant impact on the  
224 surrounding area of the sampling site (Yadav, et al. 2019). C<sub>4</sub>-C<sub>5</sub> alkanes and some  
225 aromatics were the main tracers of motor vehicle exhaust, (Fan et al., 2021). However,  
226 those species were cut down in 2020, which might be affected by the epidemic. As a  
227 tracer of coal burning, acetylene was gradually decreased from 4.3±4.3 ppbv in 2018  
228 to 0.7±0.8 ppbv in 2020.

### 229 **3.1.3 Seasonal variations**

230 As plotted in Fig. S2 and Table S3, the monthly mean mixing ratios of VOCs  
231 and its compounds were investigated. VOCs showed a clear seasonal dependence with  
232 a highest concentration in winter (50.0 ppbv) followed by spring (38.4 ppbv), autumn



233 (32.5 ppbv) and summer (26.1 ppbv). Meanwhile, the seasonal variations in the group  
234 of alkanes, alkenes, alkynes, and aromatics were similar to VOCs. In addition, the  
235 monthly mean mixing ratios of dominant and tracer species were plotted in Fig. 2.  
236 The results showed that almost all VOCs had a clear seasonal dependence, which  
237 were shown as highest concentration in winter while lowest concentration in summer.  
238 However, the mixing ratios of isoprene were highest (0.82 ppbv) in July and lowest  
239 (0.11 ppbv) in December. As the tracer of biogenic source, isoprene showed a positive  
240 correlation with temperature ( $R^2=0.61$ ,  $p<0.01$ ). Besides biogenic emission, the  
241 seasonal VOC variation was mainly influenced by the changes of anthropogenic  
242 sources. As a northern city of China, Zhengzhou emits a lot of pollutants during the  
243 heating season in winter (Wang et al., 2019). The higher concentration of VOC and  
244 tracers (such as acetylene and aromatics) in winter may be derived from coal  
245 combustion (Zhang et al., 2020).

246 Seasonal variations in VOCs concentrations were associated with several factors,  
247 such as photochemical activities and meteorological conditions. In summer, VOC is  
248 consumed under the condition of high temperature, strong light radiation, and high  
249 concentration of OH radicals (Huang et al., 2019). In winter, the high level of VOCs  
250 can be attributed to lower boundary layer and calm weather conditions (Hui et al.,  
251 2019). In addition, the pollution transmission from BTH region cannot be ignored  
252 because that the north wind prevails in Zhengzhou in winter. The seasonal variation of  
253 VOCs in several cities was investigated and the variation trend of VOC  
254 concentrations in most studies were similar to that in Zhengzhou (Liu, et al., 2019;  
255 Yadav et al., 2019).

### 256 3.1.4 Diurnal variations

257 The diurnal variations in VOCs, trace gases ( $\text{NO}_2$  and  $\text{O}_3$ ), and meteorological  
258 parameters (T, RH, WS, and UV) are shown in Fig.S3. The VOCs presented a reverse  
259 trend with  $\text{O}_3$  ( $R^2=-0.82$ ,  $p < 0.01$ ), whereas the diurnal variation in VOCs showed  
260 moderate consistency with the variations of  $\text{NO}_2$  ( $R^2= 0.62$ ,  $p < 0.01$ ). The high values



261 of VOCs generally appeared in the morning with low O<sub>3</sub> concentrations. The peak in  
262 the morning was attributed to vehicle emission (Li et al., 2019b). In addition, local  
263 meteorology and atmospheric processes also played important roles in the diurnal  
264 variations of VOCs in ambient air. In the early morning, VOC remained at a high  
265 concentration due to the stable atmospheric condition and shallow boundary layer  
266 height (Hui et al., 2020). The value of VOCs declined to the lowest value (26.7 ppbv)  
267 at 15:00 China standard time (CST), in which O<sub>3</sub> reached a maximum level as the  
268 production rate of O<sub>3</sub> and the consumption rate of O<sub>3</sub> reached equilibrium. In the  
269 afternoon, high temperature and light radiation intensity led to the consumption of  
270 VOCs. Meanwhile, higher wind speed also accelerated the diffusion of VOCs.  
271 Afterward, VOC concentration gradually accumulated with the arrival of the late  
272 traffic peak, and keep a high level throughout the night. It should be noted that VOC  
273 concentrations at night were generally higher than those during the day. Previous  
274 studies have suggested that VOC can be oxidized by O<sub>3</sub>, OH radicals and NO<sub>3</sub>  
275 radicals (Atkinson and Arey, 2003). During the daytime, the reactions with OH  
276 radicals and O<sub>3</sub> are the most important chemical reactions for VOCs, while the  
277 reactions with NO<sub>3</sub> radicals and O<sub>3</sub> are the main sedimentation reactions occurring at  
278 night. VOCs concentrations were generally higher at night because the chemical  
279 activity of OH radicals is much higher than that of NO<sub>3</sub> radicals (Carter, 2010).

280 The mean diurnal variations of high concentration and tracer VOCs were  
281 investigated, as shown in Fig. 3. As tracers of motor vehicle exhaust (Zheng, et al.  
282 2018), Iso/n-pentane had a remarkable peak at 8:00 CST, which is suggested to be  
283 vehicle emissions. Meanwhile, BTX and C<sub>2</sub>-C<sub>4</sub> alkanes also represented similar  
284 diurnal variation characteristics, which was speculated to be greatly affected by motor  
285 vehicles. However, the mixing ratio of isoprene showed higher values in the afternoon  
286 and had a similar trend with temperature. The elevated values of isoprene in the  
287 afternoon indicated significant emissions from biogenic sources.



### 288 3.2 Diagnostic ratios

289 Some of the VOC species are commonly used as indicators for emission sources.  
290 To characterize the differences in the contribution of various sources in four seasons,  
291 the ratio of B/T (benzene/toluene) and *i*-pentane / *n*-pentane have been used as the  
292 preferred metric in this study.

293 The ratio of B/T can be used to distinguish potential sources such as traffic  
294 emission, coal+biomass combustion and solvent usage. Diagnostic ratios varied  
295 according to the emission sources (i.e., below 0.20 for solvent usage, 0.5 for traffic  
296 source, 1.5-2.2 for coal combustion, and 2.5 for biomass burning). (Huang et al., 2019;  
297 Li et al., 2019a). As shown in Fig. S4, the highest value of the B/T ratio was 0.55 in  
298 winter, suggesting traffic emissions had affected the atmosphere. Meanwhile, the  
299 ratios are 0.31, 0.27, and 0.31 in spring, summer, and autumn, respectively, indicating  
300 it is more likely the aromatic derived from the mixed sources of solvent usage and  
301 vehicle source during these seasons. As a transportation hub, Zhengzhou has a large  
302 number of motor vehicles (Gu et al., 2019a). Therefore, the region needs to strengthen  
303 the control of motor vehicle.

304 The ratio of *i*-pentane to *n*-pentane was also investigated. *i*-Pentane and  
305 *n*-pentane have similar reaction rates with the OH radicals and the ratios of these pair  
306 species indicated different sources. Pentanes always originated from the consumption  
307 of coal combustion, vehicle emissions, and fuel evaporations with the ratio range of  
308 0.56–0.80, ~ 2.2, and 3.8, respectively (Huang et al., 2019; Li et al., 2019a). The  
309 highest ratio of *i*-pentane / *n*-pentane was found in summer (2.79), indicating strong  
310 impacts of traffic sources. The ratio was 1.88 in spring and 1.96 in autumn, which  
311 suggested that most of VOCs originated from the mixed sources of vehicle emissions  
312 and coal combustion. In addition, the average ratios in winter (1.55) was lower than  
313 the other three seasons, indicating the comparatively stronger contribution from coal  
314 burning in the heating season.



### 315 **3.3 Source apportionment by PMF model**

#### 316 **3.3.1 Source identification**

317 Six sources, namely industrial sources, solvent use, vehicle exhaust, LPG/NG,  
318 coal+biomass burning and biogenic sources were identified by the PMF model. The  
319 source profiles of VOCs during the sampling period are presented in Fig.4.

320 Both sources 1 and 2 were characterized by a high percentage of C<sub>6</sub>-C<sub>8</sub> alkanes  
321 and aromatics, which were major components emitted from various solvents or  
322 industrial processes (Zhou et al. 2019, Wang et al. 2021). However, source 1 was also  
323 rich in ethylene and propylene, which indicated the raw materials or products of  
324 chemical manufacturing processes (Fan et al. 2021, Hui et al. 2021). In addition, this  
325 source had correlations with gas tracers of NO<sub>2</sub>, SO<sub>2</sub>, and CO (R<sup>2</sup>=0.42, 0.37, and  
326 0.44, respectively). Meanwhile, source 2 appeared to exhibit poor correlations with  
327 gas tracers (R<sup>2</sup><0.10). Therefore, source 1 was assigned to industrial sources, while  
328 source 2 was identified as solvent use.

329 Source 3 contained higher levels of C<sub>4</sub>-C<sub>6</sub> alkanes and aromatic. It is reported  
330 that i-pentane were usually originated from gasoline evaporation (Mo et al. 2017), and  
331 the other species are all associated with vehicle exhausts (Zheng et al. 2021). A ratio  
332 of T/B was 2.0 in this profile, which further confirmed the effect of vehicular  
333 emissions (Yao et al. 2021). In addition, the source correlated significantly with CO  
334 and NO<sub>2</sub> (p<0.01), but not with SO<sub>2</sub> (p>0.05). Therefore, source 3 was identified as  
335 vehicle exhaust.

336 Source 4 was dominated by a strong presence of ethane, propane, propylene, and  
337 i/n-butane, which can also release from fuel evaporation (gasoline and LPG/NG)  
338 (Zhang et al. 2019). In particular, the aromatics of this source were very low. Similar  
339 to factor 3, the source did not correlate with SO<sub>2</sub> (p>0.05), but had a positive  
340 correlation with CO and NO<sub>2</sub> (p<0.01). Therefore, this source was considered as  
341 LPG/NG.

342 The fifth source was distinguished by significant amounts of acetylene (72%),



343 which is a marker of combustion sources (Hui et al. 2021). In addition, the source was  
344 also characterized by a significant amount of benzene and C<sub>2</sub>-C<sub>3</sub> hydrocarbons, which  
345 are representative species of coal and biomass burning (Zheng et al. 2021).  
346 Meanwhile, the independent traces (i.e., NO<sub>2</sub>, SO<sub>2</sub>, and CO) exhibited correlations  
347 with this factor ( $p < 0.01$ ,  $R^2 > 0.3$ ). Therefore, source 5 was considered to be  
348 coal+biomass burning.

349 Source 6 exhibited a significantly high composition of isoprene, which mainly  
350 produced by vegetation through photosynthesis (Song et al. 2019a). Accordingly,  
351 source 6 was labeled as biogenic source.

### 352 **3.3.2 Inter-annual variation**

353 The concentration contributions of each VOC source during 2018-2020 are  
354 shown in Fig.5. In 2018, vehicular exhaust was the largest contributor to VOC mixing  
355 ratios (28%), followed by solvent utilization (27%), LPG/NG (17%) and industrial  
356 sources (15%). The contribution of coal+biomass burning and biogenic source  
357 accounted for 8% and 5% of the total VOC concentration, respectively. As for 2019,  
358 vehicle emissions made the largest contribution (33%) to atmospheric VOCs. The  
359 second most significant source was solvent utilization, accounting for 24% of the total.  
360 The contribution of LPG/NG, industrial sources, coal+biomass burning, and biogenic  
361 source to atmospheric VOCs were 16%, 14%, 10% and 3% in 2019. While vehicular  
362 exhaust, solvent use, LPG/NG, industrial sources, coal+biomass burning and biogenic  
363 source occupied 33%, 21%, 20%, 13%, 9% and 4% in 2020, respectively.

364 In summary, vehicle emissions, solvent use and LPG/NG made the largest  
365 contributions in all three years. Meanwhile the proportion of vehicle emissions and  
366 LPG/NG has increased with each passing year. As a famous transportation hub city,  
367 the number of motor vehicles in Zhengzhou maintain the annual growth of 0.4 million  
368 during the past five years, and has exceeded 4.5 million in 2020 (Gu et al., 2019a).  
369 Thus, vehicle exhaust was an important source of ambient VOCs at Zhengzhou.  
370 LPG/NG are widely used in residential life, industrial production, and motor vehicle.



371 Combined with the actual situation of the site, residential emissions may be the main  
372 source of LPG/NG. With the adjustment of energy structure, most industrial  
373 enterprises and taxis in Zhengzhou have used NG as energy or fuel. It should be  
374 pointed out that the proportion of industrial and solvent sources presented an annual  
375 down trend. In recent years, Zhengzhou City has carried out special actions for VOC  
376 emission reduction, focusing on the control of industrial and small scattered pollution  
377 enterprises. According to the results of the PMF model, it is speculated that the effect  
378 of policy control is remarkable.

379 The source contributions determined in this study were also compared with other  
380 researches. Table 2 shows the source apportionment of VOCs was basically within the  
381 values reported for other Chinese cities (Huang et al., 2019; Hui et al., 2018; Li et al.,  
382 2020c; Mo et al., 2017; Yan et al., 2017). It was found that traffic emission is the  
383 main source of VOCs in Zhengzhou and other seven cities, which indicated that  
384 vehicle emission has a great impact on the concentration of VOCs in urban  
385 atmosphere. It should be noted that the contributions of each source in this study were  
386 very similar to those of Wuhan (Hui et al., 2018). Considering that Zhengzhou and  
387 Wuhan are both important transport hub cities in Central China, the result is in line  
388 with expectations.

### 389 **3.3.3 Seasonal variation**

390 Due to the different meteorological conditions and emission strengths, source  
391 contributions were variable in different seasons. As shown in Fig.6, the seasonal  
392 variations of biogenic emissions were significant, with the high contribution in  
393 summer (8%) and the lowest value in winter (<1%). This might be affected by both  
394 temperature and light intensity. Contrarily, the contributions from coal+biomass  
395 burning and LPG/NG were larger in winter and lower in summer. Combustion  
396 sources accounted for a larger proportion of emissions in winter (14%), while only  
397 4% in summer. It should be pointed out that LPG accounted for a relatively high  
398 concentration in winter along with the continuous promotion of coal to gas conversion.



399 Meanwhile, industrial emissions contributed to a high percentage of the VOCs in  
400 spring (21%) but exhibited a low value in autumn (12%). In addition, motor vehicle  
401 emissions have no obvious seasonal characteristics, and the contribution rate to the  
402 atmosphere in four seasons exceeded 20% of the VOCs, indicating that motor  
403 vehicles had a great impact on the air quality of Zhengzhou.

#### 404 **3.3.4 CPF and daily variation of each source**

405 To examine the source orientation and time series of each source, CPFs and  
406 diurnal variation are provided in Fig. 7.

407 CPF plots indicated the biogenic sources mainly originated from the north  
408 direction with conditional probability (CP) values of approximately 0.37. It is mainly  
409 affected by the plant emission in the northern suburbs and the urban greening in the  
410 sampling area. In addition, the diurnal patterns of biogenic source showed an obvious  
411 T dependence, with the highest concentration at midday, might due to photosynthesis  
412 activity. The CPF plots also showed coal+biomass burning and industrial source  
413 originated from the northeast and south direction. The diurnal variation in combustion  
414 source was characterized by an apparent increase at night, which is related to the  
415 accumulation of pollutants during night heating. Moreover, the highest VOC  
416 concentration from the industrial source was observed at 10:00 CST, probably due to  
417 the industrial activities during the daytime. CPF plots for solvent use indicated these  
418 sources were located at the southeast of the monitoring station. Meanwhile, the  
419 LPG/NG source displayed higher contributions from the north and east direction,  
420 associated with resident activities around the sampling site. The vehicle emissions  
421 were related to all directions, which might come from the emission of dense road  
422 network around the station. The diurnal pattern of traffic source was characterized by  
423 two peaks in the morning and evening derived from traffic rush hours.

#### 424 **3.4 AOC**

425 During the sampling periods, AOC was quantified and shown in Fig.8. The



426 calculated averaged value of total AOC was  $7.4 \times 10^7$  molecules  $\text{cm}^{-3} \text{s}^{-1}$ , which was  
427 comparable to those reported in a suburban site between Beijing and Tianjin (Yang et  
428 al., 2020b), but significantly higher than those observed in Shanghai (Zhu, et al. 2020),  
429 Hong Kong (Xue et al., 2016), Chile (Elshorbany et al., 2009) and Berlin (Geyer et al.,  
430 2001). Among AOC categories, OH exhibited the highest average concentration ( $7.0$   
431  $\times 10^7$  molecules  $\text{cm}^{-3} \text{s}^{-1}$ ), accounting for 95% of the total AOC, followed by  $\text{O}_3$  ( $3.4$   
432  $\times 10^6$  molecules  $\text{cm}^{-3} \text{s}^{-1}$ ) and  $\text{NO}_3$  ( $1.1 \times 10^5$  molecules  $\text{cm}^{-3} \text{s}^{-1}$ , which contributed  
433 to 4% of the total AOC. Thus, OH is the main contributor of the atmospheric  
434 oxidation in Zhengzhou, and similar results have been reported by other studies (Yang  
435 et al., 2021; Zhu et al., 2020).

436 During 2018-2020, the total AOC presented decreasing trend annually (as shown  
437 in Fig.8), with the mean values of 8.0, 6.4 and  $6.2 \times 10^7$  molecules  $\text{cm}^{-3} \text{s}^{-1}$ ,  
438 respectively. As expected, OH was the predominant oxidant in all three years, with  
439 95%, 95% and 97% of the total AOC, respectively. The primary pollutants (eg., CO,  
440  $\text{CH}_4$ , and VOCs) decreased significantly in 2020 due to large reductions in economic  
441 activities and associated emissions in COVID-19 lockdown. However, the average  
442 concentration of OH was highest in 2020 ( $4.8 \times 10^7$  molecules  $\text{cm}^{-3}$ ), which is far  
443 higher than that of the previous two years. Thus, the level of atmospheric oxidation  
444 needed additional attention. It should be noted the oxidation of the atmosphere has not  
445 decreased or even increased significantly during the epidemic, which has been  
446 reported by many researches (Wang et al., 2021b).

447 As shown in Fig. S5, the mean AOC values showed pronounced seasonal  
448 variations. The highest total AOC value was detected in summer ( $7.5 \times 10^7$  molecules  
449  $\text{cm}^{-3} \text{s}^{-1}$ ), followed by winter ( $6.4 \times 10^7$  molecules  $\text{cm}^{-3} \text{s}^{-1}$ ), spring ( $5.8 \times 10^7$   
450 molecules  $\text{cm}^{-3} \text{s}^{-1}$ ) and autumn ( $5.7 \times 10^7$  molecules  $\text{cm}^{-3} \text{s}^{-1}$ ). The concentration of  
451 OH in summer was significantly higher than that in other seasons, which can be  
452 ascribed to relatively favorable meteorological conditions. Meanwhile, the high  
453 isoprene concentrations were observed in summer, and its high reaction rate  
454 coefficients with the oxidants (eg., OH,  $\text{NO}_3$  and  $\text{O}_3$ ) revealed a highly oxidative  
455 environment during the summer campaign in Zhengzhou. This seasonal pattern of the



456 AOC were similar with those of other studies conducted at the national level, urban  
457 and suburban environments (Yang et al., 2021; Li et al., 2020a).

### 458 **3.5 Atmospheric environmental implications**

#### 459 **3.5.1 OH reactivity of measured species**

460 The calculated OH reactivity was categorized into SO<sub>2</sub>, NO<sub>2</sub>, NO, O<sub>3</sub>, CO and  
461 VOCs and shown in Fig.9. During the sampling period, the average values of the total  
462 OH reactivity was 45.3 s<sup>-1</sup>. In general, the OH reactivity assessed in this paper was  
463 much higher than those determined in Shanghai (Tan et al., 2019), Chongqing (Tan et  
464 al., 2019), Shanghai (Zhu et al., 2020) and New York (Ren et al., 2006), but was  
465 comparable or lower than those in Xianghe (Yang et al., 2020a) and Backgarden (Lou  
466 et al., 2010). In Zhengzhou, NO<sub>2</sub> made the largest contribution to the total OH  
467 reactivity (54%), followed by VOCs (17%), NO (16%), CO (11%), SO<sub>2</sub> (3%) and O<sub>3</sub>  
468 (1%). Similar results have also been reported in previous studies conducted in other  
469 regions (Yang et al., 2021). It should be pointed out that this paper only calculated the  
470 OH reactivity of measured species, but did not involve unmeasured species, such as  
471 secondary products (OVOCs and nitrates produced by photochemical reactions) and  
472 monoterpenes. Therefore, the value of OH reactivity in this study was underestimated  
473 to a certain extent.

474 The detailed contribution of each VOC group to the total OH reactivity were  
475 presented in Table S4 and Table S5. The OH reactivity of total VOCs was 8.1 s<sup>-1</sup>,  
476 which was much lower than those in Beijing (11.2 s<sup>-1</sup>) and Heshan (18.3 s<sup>-1</sup>) (Yang et  
477 al., 2017), but close to that in Xianghe (7.9 s<sup>-1</sup>) (Yang et al., 2020). The contribution  
478 of alkenes to OH reactivity was predominant, accounting for 5.2 s<sup>-1</sup> of the total OH  
479 reactivity of VOCs. During the sampling period, isoprene attained the largest  
480 contribution to the OH reactivity of the total VOCs, followed by ethene, m/p-xylene,  
481 propene, styrene, cis-2-butene, trans-2-butene, toluene, i-pentane and trans-2-pentene,  
482 collectively accounting for 70% of the OH reactivity towards the total VOCs.



483 As shown in Fig.9, the OH reactivity showed significant inter-annual and  
484 seasonal variations. The statistical results exhibit decreasing trend of OH reactivity  
485 during 2018-2020 in Zhengzhou, with the mean values of 51.1, 46.9, and 36.9 ppbv,  
486 respectively. The trend might due to emission reduction measures, such as  
487 traffic-related emissions and the “Coal to Gas” project. The OH reactivity value in  
488 2020 was 21% lower than that in the previous year, which is closely related to the  
489 emission reduction as a result of COVID-19. As for seasonal variations, the mean  
490 values were in the order of winter ( $74.5 \text{ s}^{-1}$ ) > autumn ( $48.6 \text{ s}^{-1}$ ) > spring ( $43.1 \text{ s}^{-1}$ ) >  
491 summer ( $29.0 \text{ s}^{-1}$ ). The notably difference might be attributed to the higher reactive  
492 trace gas loadings, especially in NO<sub>x</sub> and CO. As a northern city, coal combustion in  
493 heating season in Zhengzhou produces higher concentrations of NO<sub>x</sub> and CO, leading  
494 to higher OH reactivity. Therefore, we should continually strengthen the control of  
495 trace gases, especially in autumn and winter. The OH reactivity of total VOCs was  
496 close, with higher value in winter ( $7.3 \text{ s}^{-1}$ ) and lower in autumn ( $5.3 \text{ s}^{-1}$ ). However,  
497 the concentrations of key species were significantly different among the four seasons.  
498 Ethylene and propylene had highest OH reactivity in winter, which is speculated to  
499 the emission of combustion sources. In addition, Isoprene made the largest  
500 contribution to the total OH reactivity in summer and spring, proving significantly  
501 affected by biogenic source. Overall, the research on specific OH reactivity clearly  
502 elucidated the seasonal and annual variations of major reactants. Therefore, the  
503 control strategy based on OH reactivity should focus on key species.

### 504 **3.5.2 The effect of VOCs on ozone formation**

505 Since VOCs are important precursors of O<sub>3</sub> formation in the ground-level  
506 atmosphere, it is necessary to adequately estimate the contribution of each VOC  
507 species to ozone formation. Fig. S6 shows the concentration contributions of the four  
508 VOCs categories expressed on different scales from 2018 to 2020. The result  
509 suggested aromatics made the largest contribution of the MIR concentration,  
510 accounting for the combined ratios of 81%. Meanwhile, alkenes were the largest



511 contributors to PE concentration (87%). Although the concentrations of aromatics and  
512 alkenes were relatively low, these two VOC groups played an important role in ozone  
513 formation. This result is supported by many previous studies (Hui et al.,2021; Li et al.,  
514 2020b).

515 Among the top 10 reactive species contributed to Propy-Equiv and MIR  
516 weighted concentrations (as shown in Fig.10), eight compounds were the same,  
517 differing only in their rank order. The top 10 VOCs obtained from the two methods  
518 represented 67% and 74% of VOCs respectively. Considering the kinetic activity,  
519 isoprene ranked first with the PE method of 8.8 ppbC, accounting for approximately  
520 20% of the total PE concentration. m,p-Xylene, styrene, ethene, and toluene ranked  
521 the second to fifth based on the PE method, explaining 16%, 10%, 7%, and 5% of the  
522 total OFP, respectively. In comparison, ethene, m,p-xylene, toluene, propane, and  
523 isoprene had highest MIR concentrations, which accounted for about 23%, 21%, 12%,  
524 7%, and 7%, respectively. The results in this study highlighted the contributions of  
525 isoprene ethene, m, p-xylene, and toluene to the ozone formation, and these three  
526 species are mainly emitted from vehicle exhaust and industrial coatings (Xiong and  
527 Du, 2020).

528 Based on the results of source apportionment, the source contributions to OFP  
529 and PE were calculated (shown in Fig. S7). Vehicle emission made the greatest  
530 contribution to ozone formation, followed by solvent utilization (PE:25%; OFP:29%).  
531 Besides, the contribution of biogenic emissions cannot be ignored, occupying 23% of  
532 total PE. As the result of the discrepancy between the MIR weighted and PE weighted  
533 concentrations, the contribution of this source to OFP was relatively low, only  
534 accounting for 7%. The PE concentration method only considers the kinetic reactivity  
535 of VOC species but ignores the mechanism reactivity, while the MIR method takes  
536 the ratio of VOC/NO<sub>x</sub> on the ozone formation into consideration.

## 537 4. Conclusions

538 In this study, the hourly data of 57 VOC species were collected during 2018 to



539 2020 at an urban site in Zhengzhou, China. The results showed that the average total  
540 VOC mixing ratios were  $38.2 \pm 15.6$  ppbv, and the VOC concentrations were  
541 dominated by alkanes (60.2%) among the three years. During the sampling period, the  
542 inter-annual variation of VOCs gradually reduced as follows:  $45.0 \pm 25.2$  ppbv (in  
543 2018),  $36.7 \pm 22.0$  ppbv (in 2019), and  $30.5 \pm 15.4$  ppbv (in 2020). VOCs showed a  
544 clear seasonal dependence with the highest in winter (50.0 ppbv) and lowest in  
545 summer (26.1 ppbv). Based on PMF method, 6 sources were identified as vehicle  
546 exhaust (31%), solvent use (24%), LPG/NG (18%), industrial sources (14%),  
547 coal+biomass burning (9%) and biogenic source (4%). The proportion of vehicle  
548 emissions and LPG/NG has increased with each passing year. However, the  
549 proportion of industrial and solvent sources presented a decreasing trend. In addition  
550 to significant inter-annual variation, the sources of VOCs also showed seasonal  
551 differences. As for vehicle emissions, the contribution to the atmosphere in four  
552 seasons was more than 20%. VOCs are significantly affected by combustion sources  
553 (14%) in winter, while the influence of plant sources cannot be ignored (8%) in  
554 summer.

555         Meanwhile, this paper focuses on the atmospheric environmental implications of  
556 VOCs, including AOC, the OH reactivity and OFP. During sampling periods, the  
557 campaign-averaged value of the total AOC was  $7.4 \times 10^7$  molecules  $\text{cm}^{-3} \text{s}^{-1}$ , and OH  
558 exhibited the highest average concentration, accounting for 95% of the total AOC.  
559 The average value of the total OH reactivity was  $45.3 \text{ s}^{-1}$ , and  $\text{NO}_2$  made the largest  
560 contribution to the total OH reactivity (54%), followed by VOCs (17%), NO (16%),  
561 CO (11%),  $\text{SO}_2$  (3%) and  $\text{O}_3$  (1%). The effect of VOCs on ozone formation were  
562 investigated. Although the concentration of aromatics and alkenes were relatively low,  
563 they played an important role in ozone formation. Ethene, m, p-xylene, and toluene  
564 contributed significantly to the ozone formation in Zhengzhou. Based on the results of  
565 source apportionment, vehicle emission and solvent utilization were still key sources  
566 of VOCs that contribute to ozone formation.

567         Overall, the research of concentrations, source apportionment and atmospheric  
568 environmental implications clearly elucidated the differences in major reactants



569 observed in different seasons and years. Therefore, the control strategy should focus  
570 on key species and source among inter-annual and seasonal variations. The results can  
571 provide references for local governments to develop control strategies of VOCs  
572 during O<sub>3</sub> pollution events.  
573



## 574 **Acknowledgments**

575           This work was supported by the Study of Collaborative Control of PM<sub>2.5</sub> and  
576 O<sub>3</sub> Pollution in Zhengzhou City (No. 20200321A) and National Key Research and  
577 Development Program of China (No. 2017YFC0212403).

578

579

580

581

582



## 583 **References**

- 584 Atkinson, R., Arey, J., 2003. Atmospheric degradation of volatile organic compounds.  
585 Chem. Rev. 103, 4605-4638.
- 586 Atkinson, R., Baulch, D., Cox, R., Crowley, J., Hampson, R., Hynes, R., Jenkin, M.,  
587 Rossi, M., Troe, J., 2004. Evaluated kinetic and photochemical data for  
588 atmospheric chemistry: volume I - gas phase reactions of Ox, HOx, NOx and  
589 SOx species. Atmos. Chem. Phys. 4, 1461-1738.
- 590 Carter, W., 1994. Development of ozone reactivity scales for volatile organic  
591 compounds. J. Air Waste Manag. Assoc. 44, 881-899.
- 592 Carter, W., 2010. Development of the SAPRC-07 chemical mechanism. Atmos.  
593 Environ. 44, 5324-5335.
- 594 Elshorbany, Y., Kurtenbach, R., Wiesen, P., Lissi, E., Rubio, M., Villena, G., Gramsch,  
595 E., Rickard, A., Pilling, M., Kleffmann, J., 2009. Oxidation capacity of the city  
596 air of Santiago, Chile. Atmos. Chem. Phys. 9, 2257-2273.
- 597 Fan, M., Zhang, Y., Lin, Y., Li, L., Xie, F., Hu, J., Mozaffar, A., Cao, F., 2021. Source  
598 apportionments of atmospheric volatile organic compounds in Nanjing, China  
599 during high ozone pollution season. Chemosphere. 263, 128025.
- 600 Fu, S., Guo, M., Luo, J., Han, D., Chen, X., Jia, H., Jin, X., Liao, H., Wang, X., Fan,  
601 L., Cheng, J., 2020. Improving VOCs control strategies based on source  
602 characteristics and chemical reactivity in a typical coastal city of South China  
603 through measurement and emission inventory. Sci. Total Environ. 744, 140825.
- 604 Gao, J., Zhang, J., Li, H., Li, L., Xu, L., Zhang, Y., Wang, Z., Wang, X., Zhang, W.,  
605 Chen, Y., Cheng, X., Zhang, H., Peng, L., Chai, F., Wei, Y., 2018. Comparative  
606 study of volatile organic compounds in ambient air using observed mixing ratios  
607 and initial mixing ratios taking chemical loss into account - A case study in a  
608 typical urban area in Beijing. Sci. Total Environ. 628-629, 791-804.
- 609 Garzn, J., Huertas, J., Magaa, M., Huertas, M., Crdenas, B., Watanabe, T., Maeda, T.,  
610 Wakamatsu, S., Blanco, S., 2015. Volatile organic compounds in the atmosphere



- 611 of Mexico city. *Atmos. Environ.* 119, 415-429.
- 612 Geyer, A., Aliche, B., Konrad, S., Schmitz, T., Stutz, J., Platt, U., 2001. Chemistry and  
613 oxidation capacity of the nitrate radical in the continental boundary layer near  
614 Berlin. *J. Geophys. Res.-Atmos.* 106, 8013-8025.
- 615 Gu, X., Yin, S., Lu, X., Zhang, H., Wang, L., Bai, L., Wang, C., Zhang, R., Yuan, M.,  
616 2019a. Recent development of a refined multiple air pollutant emission inventory  
617 of vehicles in the central plains of China. *J. Environ. Sci (in China)*. 84, 80-96.
- 618 Gu, Y., Li, Q., Wei, D., Gao, L., Tan, L., Su, G., Liu, G., Liu, W., Li, C., Wang, Q.,  
619 2019b. Emission characteristics of 99 NMVOCs in different seasonal days and  
620 the relationship with air quality parameters in Beijing, China. *Ecotoxicol.*  
621 *Environ. Saf.* 169, 797-806.
- 622 Gu, Y., Liu, B., Li, Y., Zhang, Y., Bi, X., Wu, J., Song, C., Dai, Q., Han, Y., Ren, G.,  
623 Feng, Y., 2020. Multi-scale volatile organic compound (VOC) source  
624 apportionment in Tianjin, China, using a receptor model coupled with 1-hr  
625 resolution data. *Environ. Pollut.* 265, 115023.
- 626 Guo, H., Cheng, H., Ling, Z., Louie, P., Ayoko, G., 2011. Which emission sources are  
627 responsible for the volatile organic compounds in the atmosphere of Pearl River  
628 Delta. *J. Hazard. Mater.* 188, 116-124.
- 629 Hsu, C., Chiang, H., Shie, R., Ku, C., Lin, T., Chen, M., Chen, N., Chen, Y., 2018.  
630 Ambient VOCs in residential areas near a large-scale petrochemical complex:  
631 Spatiotemporal variation, source apportionment and health risk. *Environ. Pollut.*  
632 240, 95-104.
- 633 Huang, X., 2020. Evaluating the effectiveness of multiple emission control measures  
634 on reducing volatile organic compounds in ambient air based on observational  
635 data: A case study during the 2010 Guangzhou Asian Games. *Sci. Total Environ.*  
636 723, 138171.
- 637 Huang, Y., Hsieh, C., 2019. Ambient volatile organic compound presence in the  
638 highly urbanized city: source apportionment and emission position. *Atmos.*  
639 *Environ.* 206, 45-59.



- 640 Hui, L., Liu, X., Tan, Q., Feng, M., An, J., Qu, Y., Zhang, Y., Jiang, M., 2018.  
641 Characteristics, source apportionment and contribution of VOCs to ozone  
642 formation in Wuhan, Central China. *Atmos. Environ.* 192, 55-71.
- 643 Hui, L., Liu, X., Tan, Q., Feng, M., An, J., Qu, Y., Zhang, Y., Cheng, N., 2019. VOC  
644 characteristics, sources and contributions to SOA formation during haze events  
645 in Wuhan, Central China. *Sci. Total Environ.* 650, 2624-2639.
- 646 Hui, L., Liu, X., Tan, Q., Feng, M., An, J., Qu, Y., Zhang, Y., Deng, Y., Zhai, R.,  
647 Wang, Z., 2020. VOC characteristics, chemical reactivity and sources in urban  
648 Wuhan, central China. *Atmos. Environ.* 224, 117340.
- 649 Hui, L., Ma, T., Gao, Z., Gao, J., Wang, Z., Xue, L., Liu, H., Liu, J., 2021.  
650 Characteristics and sources of volatile organic compounds during high ozone  
651 episodes: A case study at a site in the eastern Guanzhong Plain, China.  
652 *Chemosphere.* 265, 129072.
- 653 Jiang, N., Duan, S., Yu, X., Zhang, R., Wang, K., 2018. Comparative major  
654 components and health risks of toxic elements and polycyclic aromatic  
655 hydrocarbons of PM<sub>2.5</sub> in winter and summer in Zhengzhou: Based on three-year  
656 data. *Atmos. Res.* 213, 173-184.
- 657 Li, B., Ho, S., Gong, S., Ni, J., Li, H., Han, L., Yang, Y., Qi, Y., Zhao, D., 2019a.  
658 Characterization of VOCs and their related atmospheric processes in a central  
659 Chinese city during severe ozone pollution periods. *Atmos. Chem. Phys.* 19,  
660 617-638.
- 661 Li, K., Li, J., Tong, S., Wang, W., Huang, R.-J., Ge, M., 2019b. Characteristics of  
662 wintertime VOCs in suburban and urban Beijing: concentrations, emission ratios,  
663 and festival effects. *Atmos. Chem. Phys.* 19, 8021-8036.
- 664 Li, Q., Badia, A., Wang, T., Sarwar, G., Fu, X., Zhang, L., Zhang, Q., Fung, J., Cuevas,  
665 C., Wang, S., Zhou, B., Saiz-Lopez, A., 2020a. Potential effect of halogens on  
666 atmospheric oxidation and air quality in China. *J. Geophys. Res-atmos.* 125,  
667 e2019JD032058.



- 668 Li, Y., Yin, S., Yu, S., Yuan, M., Dong, Z., Zhang, D., Yang, L., Zhang, R., 2020b.  
669 Characteristics, source apportionment and health risks of ambient VOCs during  
670 high ozone period at an urban site in central plain, China. *Chemosphere*. 25,  
671 126283.
- 672 Li, Q., Su, G., Li, C., Liu, P., Zhao, X., Zhang, C., Sun, X., Mu, Y., Wu, M., Wang, Q.,  
673 Sun, B., 2020c. An investigation into the role of VOCs in SOA and ozone  
674 production in Beijing, China. *Sci. Total. Environ.* 720, 137536.
- 675 Liebmann, J., Muller, J., Kubistin, D., Claude, A., Holla, R., Plass-Dülmer, C.,  
676 Lelieveld, J., Crowley, J., 2018. Direct measurements of NO<sub>3</sub> reactivity in and  
677 above the boundary layer of a mountaintop site: identification of reactive trace  
678 gases and comparison with OH reactivity. *Atmos. Chem. Phys.* 18, 12045-12059.
- 679 Liu, Y., Song, M., Liu, X., Zhang, Y., Hui, L., Kong, L., Zhang, Y., Zhang, C., Qu, Y.,  
680 An, J., Ma, D., Tan, Q., Feng, M., 2019a. Characterization and sources of volatile  
681 organic compounds (VOCs) and their related changes during ozone pollution  
682 days in 2016 in Beijing, China. *Environ. Pollut.* 257, 113599.
- 683 Liu, Y., Wang, H., Jing, S., Gao, Y., Peng, Y., Lou, S., Cheng, T., Tao, S., Li, L., Li, Y.,  
684 Huang, D., Wang, Q., An, J., 2019b. Characteristics and sources of volatile  
685 organic compounds (VOCs) in Shanghai during summer: Implications of  
686 regional transport. *Atmos. Environ.* 215, 116902.
- 687 Lou, S., Holland, F., Rohrer, F., Lu, K., Bohn, B., Brauers, T., Chang, C., Fuchs, H.,  
688 Häseler, R., Kita, K., Kondo, Y., Li, X., Shao, M., Zeng, L., Wahner, A., Zhang,  
689 Y., Wang, W., and Hofzumahaus, A., 2010. Atmospheric OH reactivities in the  
690 Pearl River Delta – China in summer 2006: measurement and model results,  
691 *Atmos. Chem. Phys.* 10, 11243-11260.
- 692 Maji, S., Beig, G., Yadav, R., 2020. Winter VOCs and OVOCs measured with  
693 PTR-MS at an urban site of India: Role of emissions, meteorology and  
694 photochemical sources. *Environ. Pollut.* 258, 113651.
- 695 Mao, J., Ren, X., Chen, S., Brune, W., Chen, Z., Martinez, M., Harder, H., Lefter, B.,  
696 Rappengluck, B., Flynn, J., Leuchner, M., 2010. Atmospheric oxidation capacity



- 697 in the summer of Houston 2006: comparison with summer measurements in  
698 other metropolitan studies. *Atmos. Environ.* 44, 4107-4115.
- 699 Mo, Z., Shao, M., Lu, S., Niu, H., Zhou, M., Sun, J., 2017. Characterization of  
700 non-methane hydrocarbons and their sources in an industrialized coastal city,  
701 Yangtze River Delta, China. *Sci. Total. Environ.* 593-594, 641-653.
- 702 Norris, G., Duvall, R., Brown, S., Bai, S., 2014. EPA Positive Matrix Factorization  
703 (PMF) 5.0 Fundamentals and User Guide, U.S. Environmental Protection  
704 Agency National Exposure Research Laboratory Research Triangle Park, NC.
- 705 Prinn, R., 2003. The cleansing capacity of the atmosphere. *Annu. Rev. Environ.*  
706 *Resour.* 28, 29-57.
- 707 Ren, Y., Ma, S., Wang, W., Yu, S., Li, Y., Zhang, R., Yin, S., 2020. Ambient VOCs  
708 characteristics, ozone formation potential, and source apportionment of air  
709 pollution in spring in Zhengzhou. *Environ. Sci (in Chinese)*. 41, 2577-2585.
- 710 Ren, X., Brune, W., Mao, J., Mitchell, M., Leshner, R., Simpas, J., Metcalf, A., Schwab,  
711 J., Cai, C., Li, Y., 2006. Behavior of OH and HO<sub>2</sub> in the winter atmosphere in  
712 New York City. *Atmos. Environ.* 40, 252-263.
- 713 Schneidemesser, E., Monks, P., Plass-Duelmer, C., 2010. Global comparison of VOC  
714 and CO observations in urban areas. *Atmos. Environ.* 44, 5053-5064.
- 715 Song, C., Liu, B., Dai, Q., Li, H., Mao, H., 2019a. Temperature dependence and  
716 source apportionment of volatile organic compounds (VOCs) at an urban site on  
717 the north China plain. *Atmos. Environ.* 207, 167-181.
- 718 Song, M., Liu, X., Zhang, Y., Shao, M., Lu, K., Tan, Q., Feng, M., Qu, Y., 2019b.  
719 Sources and abatement mechanisms of VOCs in southern China. *Atmos. Environ.*  
720 201, 28-40.
- 721 Song, S., Shon, Z., Kang, Y., Kim, K., Han, S., Kang, M., Bang, J., Oh, I., 2019c.  
722 Source apportionment of VOCs and their impact on air quality and health in the  
723 megacity of Seoul. *Environ. Pollut.* 247, 763-774.
- 724 Tan, Z., Lu, K., Jiang, M., Su, R., Wang, H., Lou, S., Fu, Q., Zhai, C., Tan, Q., Yue, D.,



- 725 Chen, D., Wang, Z., Xie, S., Zeng, L., Zhang, Y., 2019. Daytime atmospheric  
726 oxidation capacity in four Chinese megacities during the photochemically  
727 polluted season: a case study based on box model simulation, *Atmos. Chem.*  
728 *Phys.* 19, 3493-3513.
- 729 Warneke, C., 2004. Comparison of daytime and nighttime oxidation of biogenic and  
730 anthropogenic VOCs along the New England coast in summer during New  
731 England air quality study 2002. *J. Geophys. Res.* 109, D10309.
- 732 Wang, M., Lu, S., Shao, M., Zeng, L., Zheng, J., Xie, F., Lin, H., Hu, K., Lu, X.,  
733 2021a. Impact of COVID-19 lockdown on ambient levels and sources of volatile  
734 organic compounds (VOCs) in Nanjing, China. *Sci. Total Environ.* 757, 143823.
- 735 Wang, Y., Zhu, S., Ma, J., Shen, J., Wang, P., Wang, P., Zhang, H., 2021b. Enhanced  
736 atmospheric oxidation capacity and associated ozone increases during  
737 COVID-19 lockdown in the Yangtze River Delta. *Sci. Total Environ.* 768,  
738 144796.
- 739 Wang, S., Yin, S., Zhang, R., Yang, L., Zhao, Q., Zhang, L., Yan, Q., Jiang, N., Tang,  
740 X., 2019. Insight into the formation of secondary inorganic aerosol based on  
741 high-time-resolution data during haze episodes and snowfall periods in  
742 Zhengzhou, China. *Sci. Total Environ.* 660, 47-56.
- 743 Wu, F., Yu, Y., Sun, J., Zhang, J., Wang, J., Tang, G., Wang, Y., 2016. Characteristics,  
744 source apportionment and reactivity of ambient volatile organic compounds at  
745 Dinghu Mountain in Guangdong Province, China. *Sci. Total Environ.* 548-549,  
746 347-359.
- 747 Xiong, Y., Du, K., 2020. Source-resolved attribution of ground-level ozone  
748 formation potential from VOC emissions in Metropolitan Vancouver, BC. *Sci.*  
749 *Total Environ.* 721, 137698.
- 750 Xu, Z., Huang, X., Nie, W., Chi, X., Xu, Z., Zheng, L., Sun, P., Ding, A., 2017.  
751 Influence of synoptic condition and holiday effects on VOCs and ozone  
752 production in the Yangtze River Delta region, China. *Atmos. Environ.* 168,  
753 112-124.



- 754 Xue, L., Gu, R., Wang, T., Wang, X., Saunders, S., Blake, D., Louie, P., Luk, C.,  
755 Simpson, I., Xu, Z., Wang, Z., Gao, Y., Lee, S., Mellouki, A., Wang, W., 2016.  
756 Oxidative capacity and radical chemistry in the polluted atmosphere of Hong  
757 Kong and Pearl River Delta region: analysis of a severe photochemical smog  
758 episode. *Atmos. Chem. Phys.* 16, 9891-9903.
- 759 Yadav, R., Sahu, L., Tripathi, N., Pal, D., Beig, G., Jaaffrey, S., 2019. Investigation of  
760 emission characteristics of NMVOCs over urban site of western India. *Environ.*  
761 *Pollut.* 252, 245-255.
- 762 Yan, D., Lei, Y., Shi, Y., Zhu, Q., Li, L., Zhang, Z., 2018. Evolution of the  
763 spatiotemporal pattern of PM<sub>2.5</sub> concentrations in China – A case study from the  
764 Beijing-Tianjin-Hebei region. *Atmos. Environ.* 183, 225-233.
- 765 Yan, Y., Peng, L., Li, R., Li, Y., Li, L., Bai, H., 2017. Concentration, ozone formation  
766 potential and source analysis of volatile organic compounds (VOCs) in a thermal  
767 power station centralized area: A study in Shuozhou, China. *Environ. Pollut.*  
768 223, 295-304.
- 769 Yang, Y., Shao, M., Keßel, S., Li, Y., Lu, K., Lu, S., Williams, J., Zhang, Y., Zeng, L.,  
770 Nölscher, A., Wu, Y., Wang, X., Zheng, J., 2017. How the OH reactivity affects  
771 the ozone production efficiency: case studies in Beijing and Heshan, China,  
772 *Atmos. Chem. Phys.* 17, 7127-7142.
- 773 Yang, Y., Liu, X., Zheng, J., Tan, Q., Feng, M., Qu, Y., An, J., Cheng, N., 2019.  
774 Characteristics of one-year observation of VOCs, NO<sub>x</sub>, and O<sub>3</sub> at an urban site in  
775 Wuhan, China. *J. Environ. Sci. (in China)*. 79, 297-310.
- 776 Yang, Y., Wang, Y., Yao, D., Zhao, S., Yang, S., Ji, D., Sun, J., Wang, Y., Liu, Z., Hu,  
777 B., Zhang, R., Wang, Y., 2020a. Significant decreases in the volatile organic  
778 compound concentration, atmospheric oxidation capacity and photochemical  
779 reactivity during the National Day holiday over a suburban site in the North  
780 China Plain. *Environ. Pollut.* 263, 114657.
- 781 Yang, Y., Wang, Y., Zhou, P., Yao, D., Ji, D., Sun, J., Wang, Y., Zhao, S., Huang, W.,  
782 Yang, S., Chen, D., Gao, W., Liu, Z., Hu, B., Zhang, R., Zeng, L., Ge, M., Petäjä,  
783 T., Kerminen, V., Kulmala, M., Wang, Y., 2020b. Atmospheric reactivity and



- 784 oxidation capacity during summer at a suburban site between Beijing and Tianjin.  
785 Atmos. Chem. Phys. 20, 8181-8200.
- 786 Yang, Y., Wang, Y., Huang, W., Yao, D., Zhao, S., Wang, Y., Wang, Y., Ji, D., Zhang,  
787 R., Wang, Y., 2021. Parameterized atmospheric oxidation capacity and speciated  
788 OH reactivity over a suburban site in the North China Plain: A comparative study  
789 between summer and winter. Sci. Total Environ. 773, 145264.
- 790 Yao, D., Tang, G., Wang, Y., Yang, Y., Wang, L., Chen, T., He, H., Wang, Y., 2021.  
791 Significant contribution of spring northwest transport to volatile organic  
792 compounds in Beijing. J. Environ. Sci. (in China). 104, 169-181.
- 793 Zhang, F., Shang, X., Chen, H., Xie, G., Fu, Y., Wu, D., Sun, W., Liu, P., Zhang, C.,  
794 Mu, Y., Zeng, L., Wan, M., Wang, Y., Xiao, H., Wang, G., Chen, J., 2020.  
795 Significant impact of coal combustion on VOCs emissions in winter in a North  
796 China rural site. Sci. Total Environ. 720, 137617.
- 797 Zhang, G., Xu, H., Qi, B., Du, R., Gui, K., Wang, H., Jiang, W., Liang, L., Xu, W.,  
798 2018. Characterization of atmospheric trace gases and particulate matter in  
799 Hangzhou, China. Atmos. Chem. Phys. 18, 1705-1728.
- 800 Zhang, X., Yin, Y., Wen, J., Huang, S., Han, D., Chen, X., Cheng, J., 2019.  
801 Characteristics, reactivity and source apportionment of ambient volatile organic  
802 compounds (VOCs) in a typical tourist city. Atmos. Environ. 215, 116898.
- 803 Zhang, Y., Wang, X., Zhang, Z., Lu, S., Huang, Z., Li, L., 2015. Sources of C(2)-C(4)  
804 alkenes, the most important ozone nonmethane hydrocarbon precursors in the  
805 Pearl River Delta region. Sci. Total Environ. 502, 236-245.
- 806 Zheng, H., Kong, S., Xing, X., Mao, Y., Hu, T., Ding, Y., Li, G., Liu, D., Li, S., Qi, S.,  
807 2018. Monitoring of volatile organic compounds (VOCs) from an oil and gas  
808 station in northwest China for 1 year. Atmos. Chem. Phys. 18, 4567-4595.
- 809 Zheng, H., Kong, S., Yan, Y., Chen, N., Yao, L., Liu, X., Wu, F., Cheng, Y., Niu, Z.,  
810 Zheng, S., Zeng, X., Yan, Q., Wu, J., Zheng, M., Liu, D., Zhao, D., Qi, S., 2020.  
811 Compositions, sources and health risks of ambient volatile organic compounds  
812 (VOCs) at a petrochemical industrial park along the Yangtze River. Sci. Total  
813 Environ. 703, 135505.



- 814 Zheng, H., Kong, S., Chen, N., Niu, Z., Zhang, Y., Jiang, S., Yan, Y., Qi, S., 2021.  
815 Source apportionment of volatile organic compounds: Implications to reactivity,  
816 ozone formation, and secondary organic aerosol potential. *Atmos. Res.* 249,  
817 105344.
- 818 Zhou, X., Li, Z., Zhang, T., Wang, F., Wang, F., Tao, Y., Zhang, X., Wang, F., Huang,  
819 J., 2019. Volatile organic compounds in a typical petrochemical industrialized  
820 valley city of northwest China based on high-resolution PTR-MS measurements:  
821 Characterization, sources and chemical effects. *Sci. Total Environ.* 671, 883-896.
- 822 Zhu, J., Wang, S., Wang, H., Jing, S., Lou, S., Saiz-Lopez, A., Zhou, B., 2020.  
823 Observationally constrained modeling of atmospheric oxidation capacity and  
824 photochemical reactivity in Shanghai, China. *Atmos. Chem. Phys.* 20,  
825 1217-1232.
- 826 Zou, Y., Deng, X., Zhu, D., Gong, D., Wang, H., Li, F., Tan, H., Deng, T., Mai, B., Liu,  
827 X., Wang, B., 2015. Characteristics of 1 year of observational data of VOCs,  
828 NO<sub>x</sub> and O<sub>3</sub> at a suburban site in Guangzhou, China. *Atmos. Chem. Phys.* 15,  
829 6625-6636.  
830



## 831 **Figure list**

832 **Fig. 1** Locations of the sampling stations in Zhengzhou.

833 .

834 **Fig. 2** Monthly changes in the concentrations of VOCs in Zhengzhou. The upper and  
835 lower boundaries of the boxes indicate the 75th and 25th percentiles, respectively; the  
836 lines within the boxes mark the median; the whiskers above and below the boxes  
837 indicate the 90th and 10th percentiles, respectively.

838

839 **Fig. 3** Diurnal variations in VOCs compounds measured at Zhengzhou. The upper and  
840 lower boundaries of the boxes indicate the 75th and 25th percentiles, respectively; the  
841 lines within the boxes mark the median; the whiskers above and below the boxes  
842 indicate the 90th and 10th percentiles, respectively.

843

844 **Fig. 4** Source profiles and contribution percentages from each source during the  
845 observation period by PMF model (bar is a mixing ratio and dot is a percentage).

846

847 **Fig. 5** The contributions of each VOC source during 2018-2020.

848

849 **Fig. 6** Seasonal variation of source contributions to VOCs concentration.

850

851 **Fig. 7** Conditional probability function (CPF) plots of local VOC sources in  
852 Zhengzhou. The mean (dot), median (horizontal line), 25th and 75th percentiles  
853 (lower and upper box), and 10th and 90th percentiles (lower and upper whiskers) for  
854 the entire study are shown.

855

856 **Fig. 8** Comparison of the relative contributions of OH, O<sub>3</sub> and NO<sub>3</sub> of the AOC in  
857 Zhengzhou during the sampling periods.

858

859 **Fig. 9** Comparison of the relative contributions the OH reactivity in Zhengzhou .

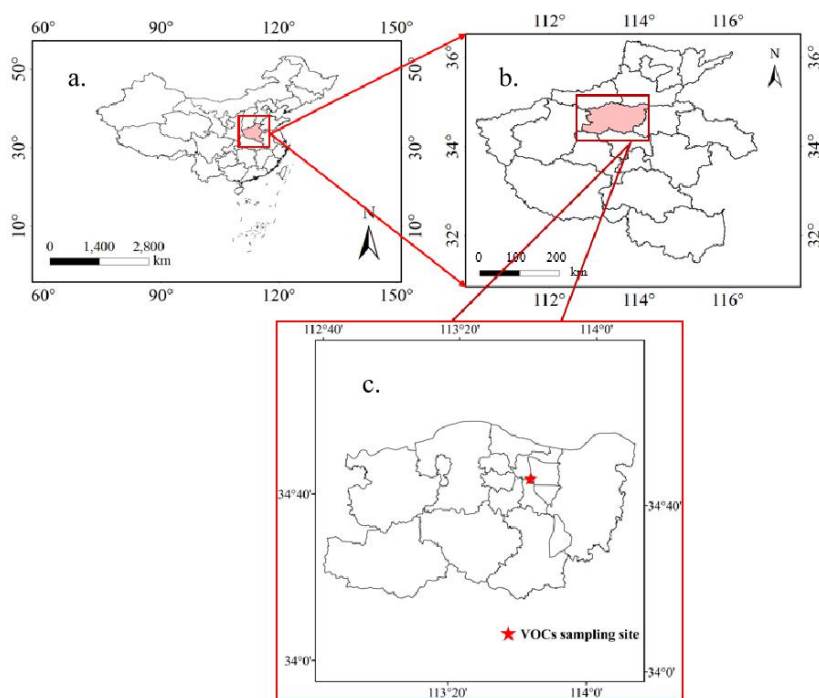
860

861 **Fig. 10** Top 10 VOCs species that contributed most to the Propy-Equiv and MIR  
862 weighted concentrations in Zhengzhou.

863



864



865

866

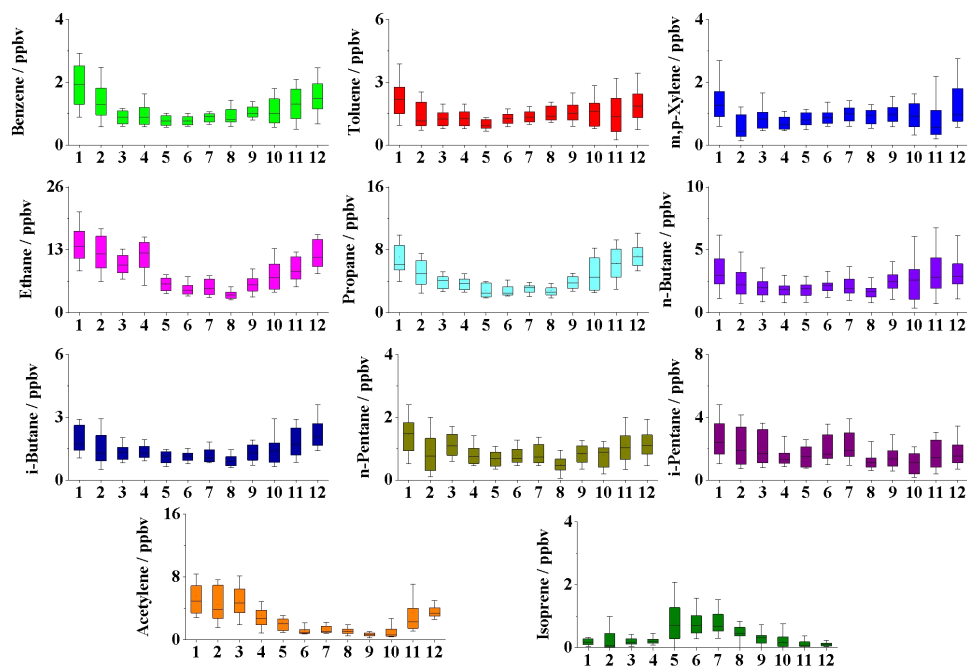
867

868

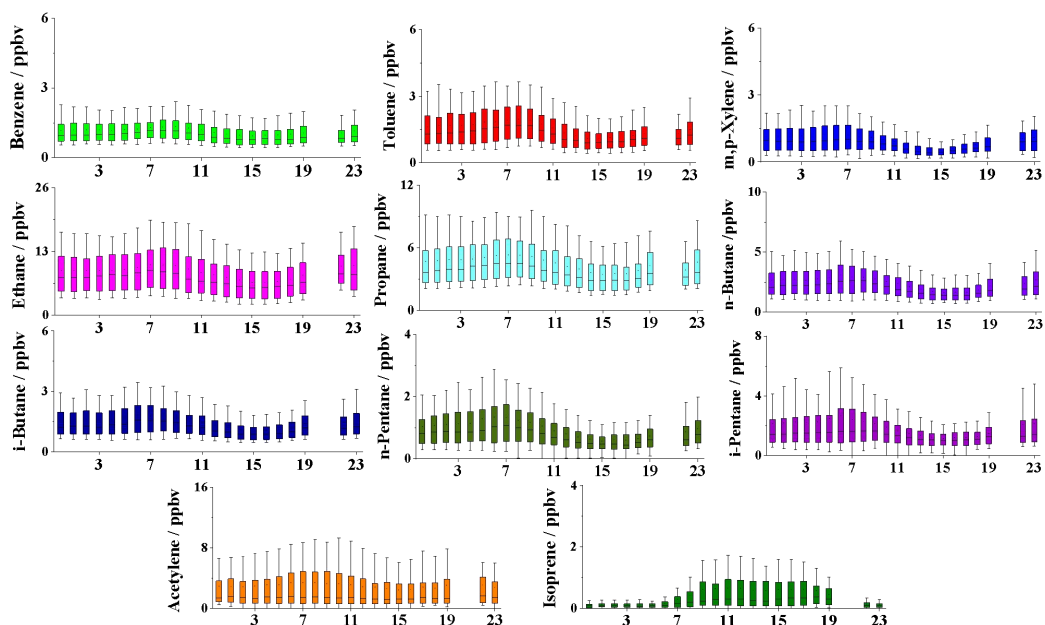
**Fig. 1** Locations of the sampling stations, and Fig. a-c represents China, Henan and Zhengzhou respectively.



869  
870  
871



872  
873 **Fig. 2** Monthly changes in the concentrations of the typical VOCs species in  
874 Zhengzhou. The upper and lower boundaries of the boxes indicate the 75th and 25th  
875 percentiles, respectively; the lines within the boxes mark the median; the whiskers  
876 above and below the boxes indicate the 90th and 10th percentiles, respectively.  
877



878

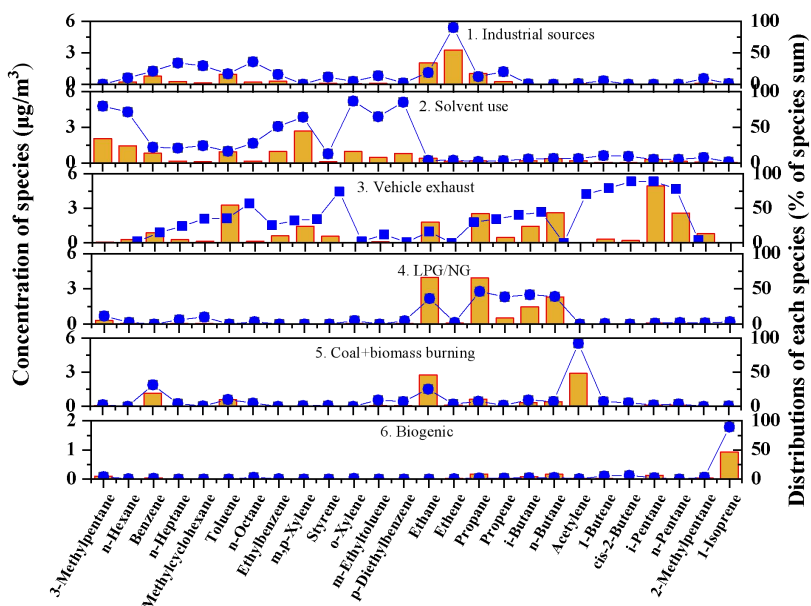
879

880 **Fig. 3** Diurnal variations in VOCs compounds measured at Zhengzhou. The upper and  
881 lower boundaries of the boxes indicate the 75th and 25th percentiles, respectively; the

882 lines within the boxes mark the median; the whiskers above and below the boxes

883 indicate the 90th and 10th percentiles, respectively.

884



885

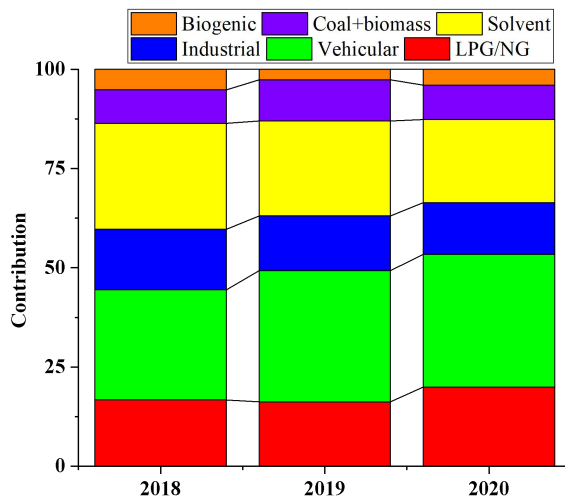
886

887

**Fig.4** Source profiles and contribution percentages during the observation period by PMF model (bar is a mixing ratio and dot is a percentage).



888



889

890

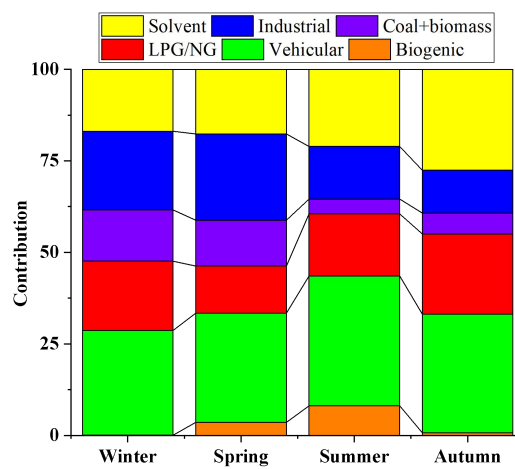
891

Fig. 5 The contributions of each VOC source during 2018-2020.



892

893

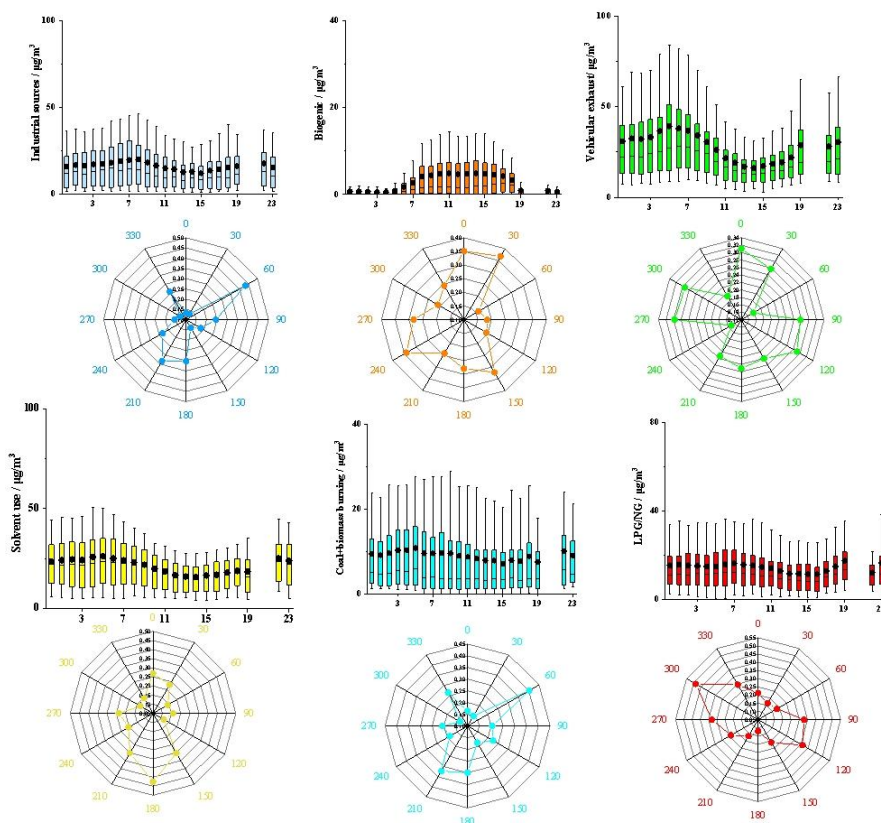


894

895

896

**Fig. 6** Seasonal variation of source contributions to VOCs concentration.

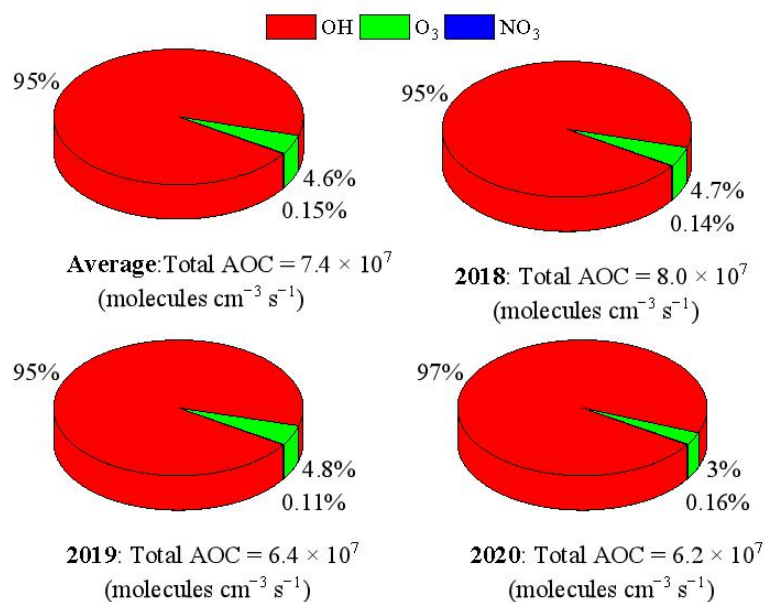


897

898

899 **Fig. 7** Conditional probability function (CPF) plots of local VOC sources in  
900 Zhengzhou. The mean (dot), median (horizontal line), 25th and 75th percentiles  
901 (lower and upper box), and 10th and 90th percentiles (lower and upper whiskers)  
902 for the entire study are shown.

903

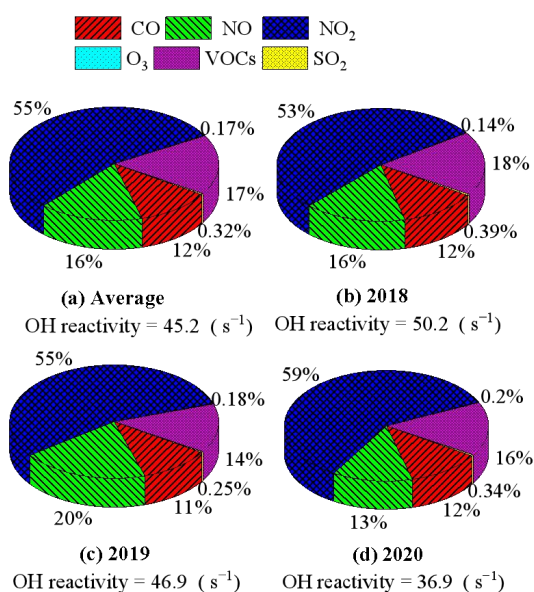


904  
905  
906  
907

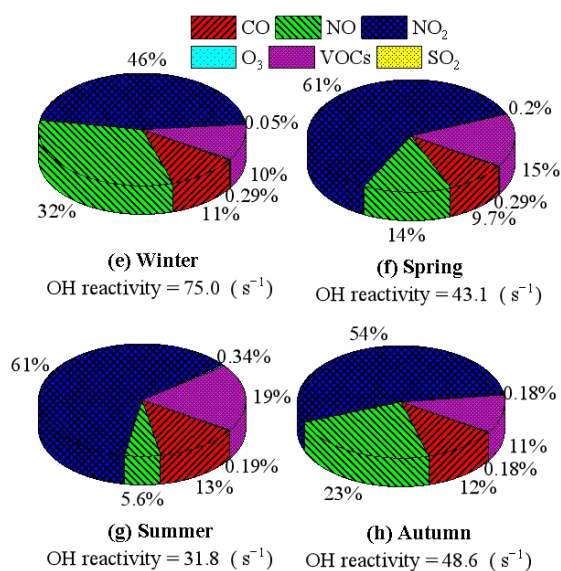
**Fig. 8** Comparison of the relative contributions of OH, O<sub>3</sub> and NO<sub>3</sub> of the AOC in Zhengzhou during the sampling periods.



908



909



910

911

912

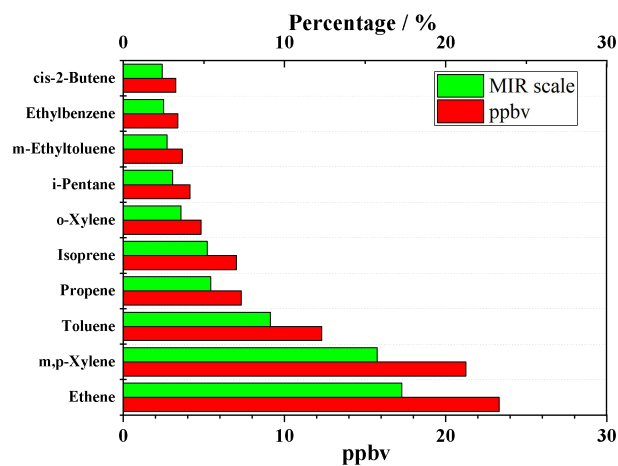
913

**Fig. 9** Comparison of the relative contributions the OH reactivity in Zhengzhou .

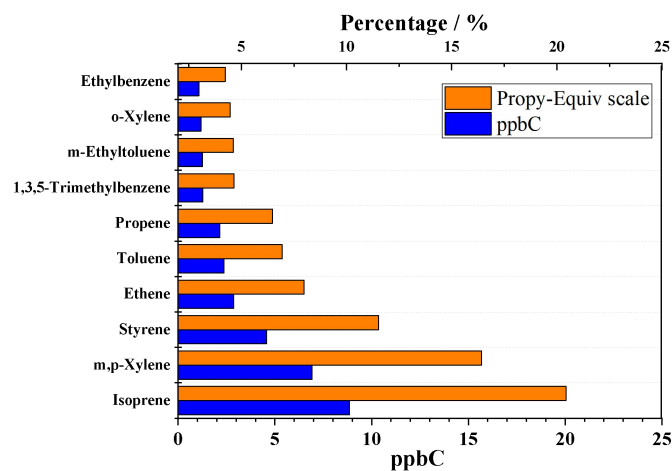


914

915



916



917

918

919

920

**Fig. 10** Top 10 VOCs species that contributed most to the Propy-Equiv and MIR weighted concentrations in Zhengzhou.



921 **Table list:**

922

923

924

925 **Table 1** Top 20 most abundant VOC species (ppbv) measured in Zhengzhou for the  
926 study period 2018-2020.

927

928 **Table 2** Comparison of source contributions resolved by PMF models in different  
929 cities.

930



931 **Table 1** Top 20 most abundant VOC species (ppbv) measured in Zhengzhou for the  
 932 study period 2018-2020.

Species	2018	Species	2019	Species	2020	Species	Average
Ethane	10±5.6	Ethane	8.7±5.7	Ethane	7.6±3.9	Ethane	8.8±5
Ethene	6±5	Propane	4.5±2.8	Ethene	3.8±2.5	Ethylene	4.7±4
Propane	4.4±2.7	Ethene	3.5±4.3	Propane	3.7±2	Propane	4.2±2.5
Acetylene	4.3±4.3	Acetylene	2.9±4.2	n-Butane	2.1±1.4	Acetylene	2.6±3.3
n-Butane	2.3±1.4	n-Butane	2.4±1.8	i-Pentane	1.4±1.4	n-Butane	2.3±1.7
i-Pentane	2.0±1.7	i-Pentane	2.1±2.0	i-Butane	1.4±0.9	Isopentane	1.9±2
Toluene	1.9±1	Toluene	1.5±1.1	Toluene	1.4±1.1	Toluene	1.6±1.1
n-Pentane	1.3±1.5	i-Butane	1.5±1.1	Benzene	1±0.5	Isobutane	1.3±1
i-Butane	1.2±0.8	Benzene	1.1±0.7	m,p-Xylene	0.9±1.1	n-Pentane	1.2±1.1
Benzene	1.2±0.7	m,p-Xylene	1.1±0.9	Acetylene	0.7±0.8	Benzene	1.1±0.6
m,p-Xylene	1.1±0.6	n-Pentane	1.1±0.9	n-Pentane	0.7±0.9	m,p-Xylene	1±1
Cyclopentane	0.9±1.0	Propene	0.8±1	Propene	0.6±1.2	Propylene	0.7±1.1
Propene	0.8±0.5	3-Methylpentane	0.6±0.4	1-Isoprene	0.4±0.5	Cyclopentane	0.7±1.1
Ethylbenzene	0.7±0.4	n-Hexane	0.6±0.6	Ethylbenzene	0.4±0.4	Isoprene	0.6±0.9
Isoprene	0.6±0.5	Ethylbenzene	0.4±0.3	Styrene	0.2±0.4	Ethyl benzene	0.5±0.4
3-Methylpentane	0.4±0.4	Isoprene	0.4±0.6	o-Xylene	0.2±0.3	3-Methyl pentane	0.4±0.4
o-Xylene	0.4±0.2	Cyclopentane	0.3±0.7	n-Heptane	0.2±0.3	n-Hexane	0.4±0.5
cis-2-Butene	0.4±0.8	o-Xylene	0.3±0.2	Cyclopentane	0.2±0.5	Styrene	0.3±0.3
Styrene	0.3±0.3	2-Methylpentane	0.2±0.3	m-Ethyltoluene	0.2±0.2	o-Xylene	0.3±0.3
n-Hexane	0.3±0.3	1-Butene	0.2±0.3	3-Methylpentane	0.2±0.2	Heptane	0.2±0.3
∑TOP 20 species/∑VOCs	90%		93%		90%		91%

933

934



935 **Table 2** Comparison of source contributions resolved by PMF models in different  
936 cities (%).

City	Sampling periods	Solvent use	Industrial sources	Vehicle exhaust	Combustion	LPG/NG	Biogenic sources
Taiwan <sup>a</sup>	January–December 2016	29	15	18	-	-	4
Wuhan <sup>b</sup>	September 1, 2016 to August 31, 2017		16	24	19	13	2
Shuozhou <sup>c</sup>	March and August, 2014	-	14	21	30	18	-
Ningbo <sup>d</sup>	December 2012, April 2013, July 2013, and October 2013	7	50	16	-	27	-
Beijing <sup>e</sup>	March 2016 to January 2017	16	10	19	-	12	8
This study	January 2018 to December 2020	24	14	31	9	17	4

937 (a:Huang et al., 2019; b:Hui et al., 2018; c: Yan et al., 2017; d: Mo et al., 2017; e: Li et al., 2020c.)

938